Gold dimer nanoantenna with slanted gap for tunable LSPR and improved SERS

ARTICLE *in* THE JOURNAL OF PHYSICAL CHEMISTRY C · JANUARY 2014

Impact Factor: 4.77 · DOI: 10.1021/jp409844y

THE JOURNAL OF PHYSICAL CHEMISTRY C

Article

pubs.acs.org/JPCC

Gold Dimer Nanoantenna with Slanted Gap for Tunable LSPR and Improved SERS

Sameh Kessentini,*[,†] Dominique Barchiesi,[‡] Cristiano D'Andrea,[§] Andrea Toma,[∥] Nicolas Guillot,[⊥] Enzo Di Fabrizio,[#,%] Barbara Fazio,[§] Onofrio M. Maragó,[§] Pietro G. Gucciardi,[§] and Marc Lamy de la Chapelle[⊥]

[†]Faculté des Sciences de Sfax, Sfax, Tunisia

[‡]GAMMA3 Project (UTT-INRIA), University of Technology of Troyes, Troyes, France

[§]IPCF-CNR, Istituto per i Processi Chimico-Fisici, Messina, Italy

[∥]Nanostructures Department, Istituto Italiano di Tecnologia, Genova, Italy

[⊥]Laboratoire CSPBAT, CNRS (UMR 7244), Université Paris 13, Bobigny, France

[#]PSE and BESE Divisions, King Abdullah University of Science and Technology (KAUST), Jeddah, Saudi Arabia

[%]BIONEM Lab, University of Magna Graecia, Catanzaro, Italy

Supporting Information

ABSTRACT: We focus on improving the surface-enhanced Raman scattering (SERS) of dimer nanoantenna by tailoring the shape of the coupled nanoantennas extremities from rounded to straight or slanted ones. A numerical model based on the discrete dipole approximation method—taking into account periodicity, adhesion layer, and roughness—is first validated by comparison with localized surface plasmon resonance (LSPR) and SERS experiments on round-edged dimer nanoantennas and then used to investigate the effect of the straight or slanted gap in the dimer antenna. Simulations show that both LSPR and SERS can be tuned by changing the gap slanting angle. The SERS enhancement factor can also be improved by 2 orders of magnitude compared to the one reached using a rounded gap. Therefore, the slanting angle can be used as a new control parameter in the design of SERS substrates to guarantee stronger field confinement and higher sensitivity, especially as its feasibility is demonstrated.

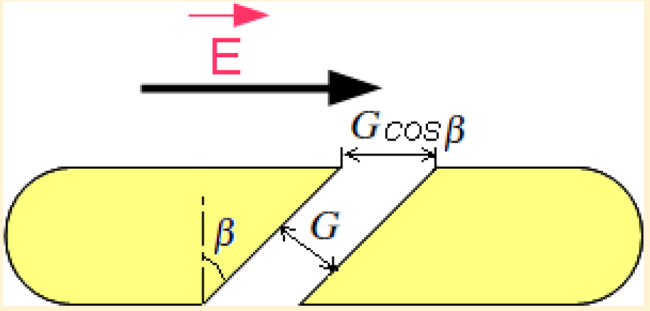

1. INTRODUCTION

Detection of small amounts of molecules for early disease diagnosis by means of plasmonic devices is currently an active research area.[1,2] Many techniques are used to get sensitive (ability to detect small amount of molecules) and selective (specific to some molecules) nanosensors based on the signal amplification provided by the localized surface plasmon resonances (LSPR) in nanostructured metallic substrates and optical nanoantennas. The detection can be based on the enhancement of the Raman signal, which provides a spectral fingerprint of the molecule to be detected, using surface-enhanced Raman scattering (SERS).[3] The detection limit can be largely improved since SERS is considered a highly sensitive technique.[4−6]

For SERS detection, molecules must be on or close to the surface of an appropriate metal substrate.[3] Currently, two classes of SERS substrates are typically used:[3] metallic nanoparticles in solution (e.g., colloidal solutions[7,8]) and planar metallic nanostructures (e.g., metallic nanoparticles supported on a planar substrate). Both exploit the resonant interaction between the conduction electrons in the metal and the incident electromagnetic field at a given wavelength (the localized surface plasmon resonance) yielding a strong electromagnetic field enhancement.[9,10] If the field enhancement is strong enough, it enables the observation of a very low amount of molecules.[11,12] The sensitivity of the SERS substrates is dependent on their geometrical features (shape and size[13−15]) and therefore can be improved by engineering these features.

Dimer-based nanoantennas, i.e. near-field coupled nanorods, are one of the most reproducible SERS planar substrates. Fischer and Martin[16] compared the dimer of bowtie to the dimer of antenna and found that the dimer antenna produces a stronger field enhancement than the bowtie for a wide range of dimers (different shapes and sizes). Moreover, the enhanced near-field reached with isolated dimer of metallic particles is

Received: October 3, 2013
Revised: January 27, 2014
Published: January 27, 2014

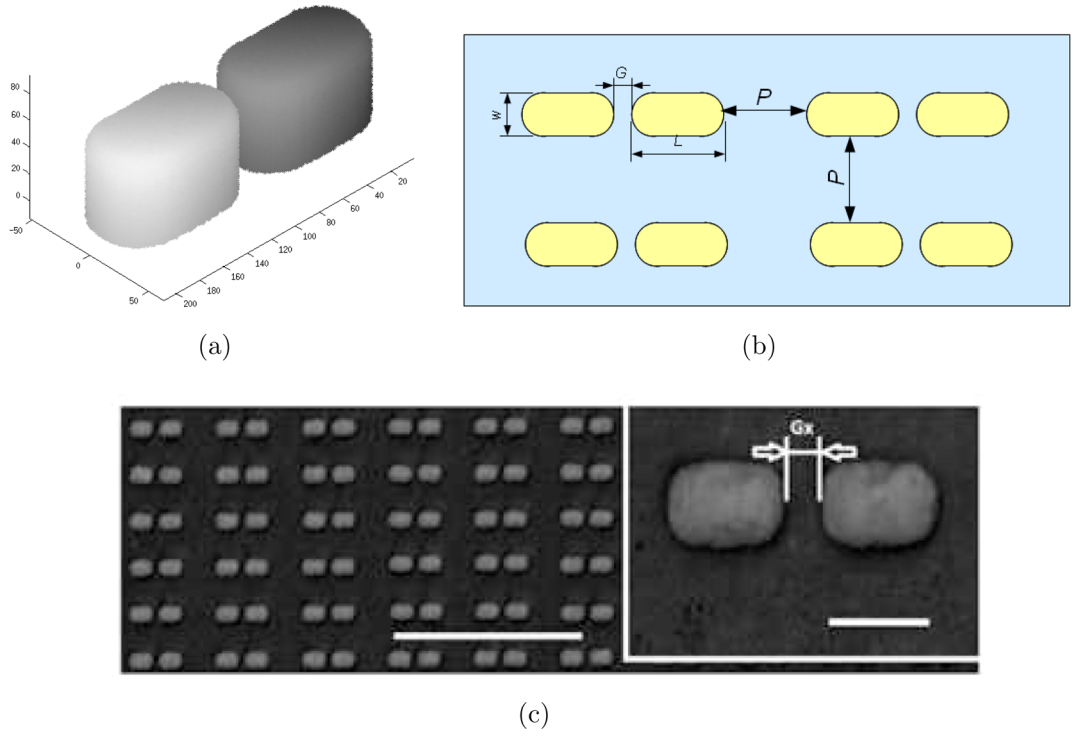

Figure 1. Periodic dimer antenna: (a) 3D view (graduations in nm), (b) upper view (P interparticle distance in both directions, G the gap size, L length, and w width of single antenna), (c) SEM scan: scale bar values are 1 μm and 100 nm, from left to right.

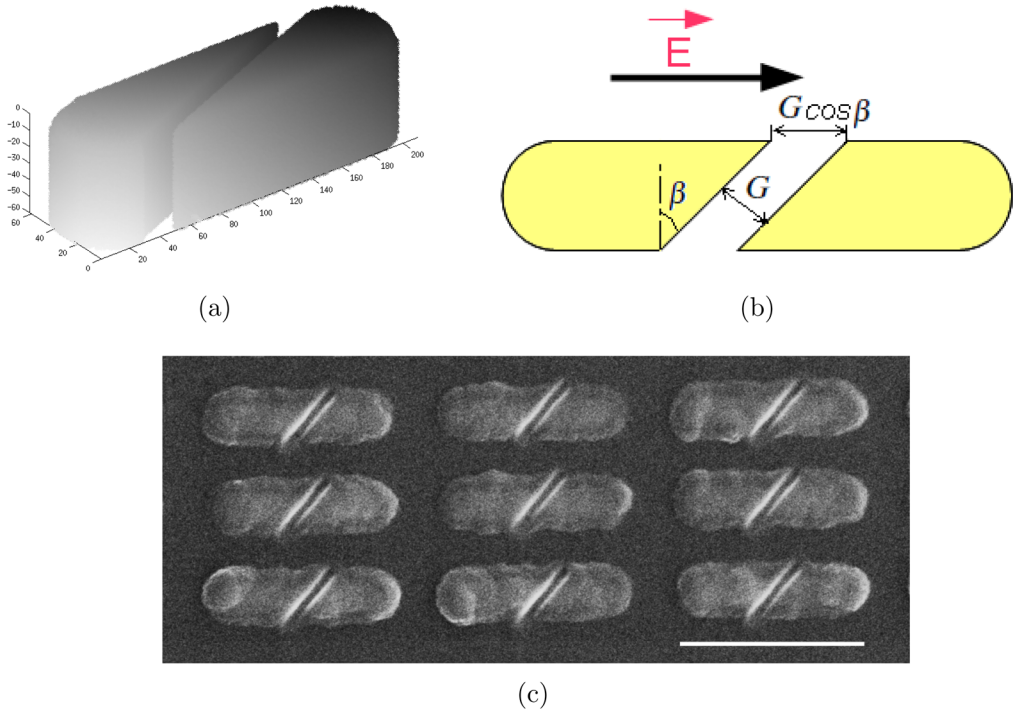

Figure 2. Dimer antenna with slanted gap: (a) 3D view (graduations in nm), (b) upper view (β is the slanting angle and G the gap distance), (c) SEM scan: scale bar value is 400 nm.

stronger than the near-field resulting if the metallic particles are part of a large array of coupled antennas.[17]

Because of improvements in the fabrication process of nanodevices, more precision is achieved[18−20] and more complicated structures can be easily fabricated.[21] These improvements motivated many studies to design new nanodevices with various shapes.[22−24] Within the above motivation, we propose a new control parameter for dimer-based nanoantenna. Originally, the structure consists of an array of dimer of gold antenna deposited via an adhesion layer on a substrate (SiO_2 or CaF_2, etc.). The dimer nanoantennas are separated by a gap with rounded edges (see Figure 1). The rounded edges result from the fabrication using the electron beam lithography (EBL).[22] However, using focused ion beam

dx.doi.org/10.1021/jp409844y | J. Phys. Chem. C 2014, 118, 3209−3219

(FIB) or helium ion lithography (HIL), a straight or slanted gap (Figure 2) can be introduced in a long nanoantenna.[25,26] This represents a new control parameter for these structures, and we have demonstrated in a preliminary study an LSPR tunability by varying the gap shape.[27]

Here, we propose a full investigation of the dependence of the slanting angle, using a numerical model based on the discrete dipole approximation (DDA). To be in relation to experiments, we first validate the model by comparison to experimental results on round-edged dimer nanoantennas. Then, simulations are carried out referring not only to LSPR but also to the near-field and the SERS enhancement factor for a range of Raman bands.

The paper is organized as follows. Section 2 describes the experiments conducted on round-edged dimer nanoantennas. Section 3 provides an overview of the numerical method and model used for the simulations. Section 4 presents the comparison of numerical results to experimental ones for validation of the model. In section 5, we suggest a sample fabrication of nanoantenna with slanted gap to demonstrate the feasibility of the structure; then the LSPR and SERS simulation results of the nanoantennas with straight or slanted gap are reported and discussed. Finally, concluding remarks are summarized in the last section.

2. EXPERIMENTS ON ROUND-EDGED DIMER NANOANTENNAS

An array of dimer antennas has been fabricated by EBL and lift-off techniques on a CaF_2 substrate with a 5 nm layer of titanium used to ensure the adhesion. The array features the following geometry (Figure 1): interparticle distance P = 200 nm, the length, width, and height of each gold antenna are respectively L = 100 nm, w = 60 nm, and h = 60 nm.

Two probe molecules have been used for comparison purposes: methylene blue (MB) and *trans*-1,2-bis(4-pyridyl)-ethylene (BPE). Extinction and SERS measurements are carried out on the same spectrometer (Horiba Jobin-Yvon HR800 for MB experiments, Horiba Jobin Yvon Xplora for BPE experiments) coupled with an Olympus B×51 optical microscope.

LSPR Peak Positions. The extinction spectra are acquired in transmission geometry (after removing the edge filters used in the Raman configuration), exciting the sample with a white xenon lamp (embedded in the microscope) whose light is first polarized with a linear polarizer, and then focused onto the sample with a condenser lens on a spot having diameter ≈100 μm (several antennas are excited). The radiation transmitted by the nanoantenna samples is collected by a 10× long working distance objective (numerical aperture, NA = 0.25), spectrally dispersed by a 600 lines/mm grating, and acquired by a Peltier-cooled CCD. As a reference signal we use the light signal transmitted through the CaF_2 substrate. The LSPR peak positions and an extinction spectra are displayed in Figure 3.

SERS Spectra. The SERS spectra are acquired in a backscattering configuration using laser diodes (λ = 785 nm, Spectra-Physics Excelsior 785) as light source. The beam is linearly polarized parallel to the dimer axis and focused on a d_{las} ≈ 700 nm diameter spot by means of a 100× objective (NA = 0.9). The laser power on the sample is 26 μW and 0.49 mW for MB and BPE, respectively, and the integration time set to 30 s for both molecules. Such parameters allow us to avoid laser-induced chemical modifications of the molecule experimentally observable with the appearance of a more and more intense

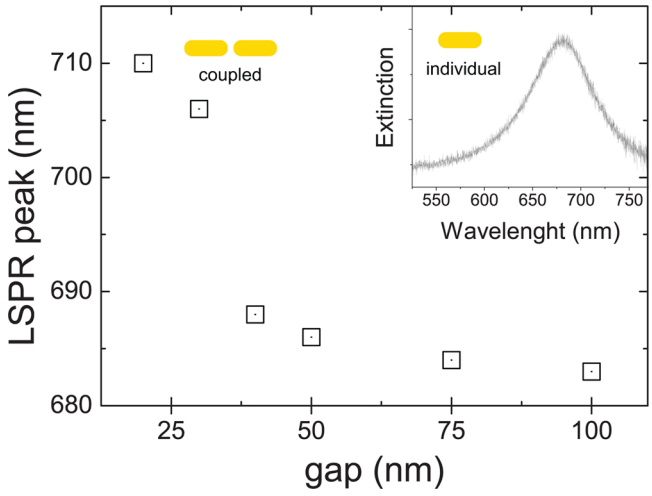

Figure 3. LSPR peak position as a function of gap distance for L = 100 nm, w = h = 60 nm nanorods. The inset displays the extinction spectrum of individual, uncoupled nanorods. The polarization of the light field is parallel to the nanorods dimer axis.

peak at 478 cm^{-1} with respect to the adjacent 445 and 501 cm^{-1} peaks and a simultaneous decrease of the overall SERS intensity.[28]

The probe molecules binding to the nanoantennas is accomplished by immersion of the antenna chip in solution (0.1 mM watery solution of MB and 1 mM of BPE) for 1 h, followed by rinsing in distilled water and drying in air. Figures 4

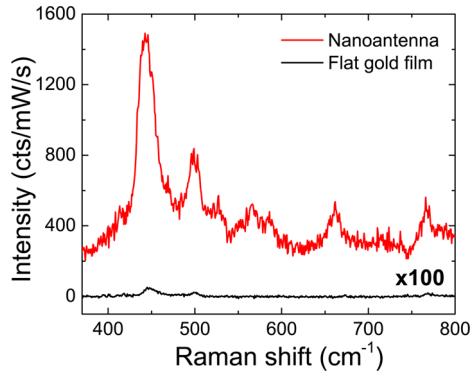

Figure 4. Red line: SERS spectrum of MB acquired on the 10 nm gap dimers sample (laser power 26 μW, inegration 30 s, the spectrum is vertically offset for clarity). Black line: Raman spectrum of MB acquired on a flat gold film (laser power 2 mW, integration 60 s, the intensity is multiplied by 100 for clarity reasons). All the spectra are normalized to laser power and integration time to make the signals directly comparable.

and 5 show the SERS spectra of MB and BPE, respectively, absorbed on the 10 nm gap dimers. The main vibrational modes of MB are clearly visible at 445 and 501 cm^{-1}, related to the CNC skeletal deformation modes.[29] A S/N ratio higher than 25 is observed for the most intense vibration. Five main features are clearly observable on the BPE SERS spectrum at 1016, 1200, 1337, 1606, and 1635 cm^{-1}. These Raman bands can been assigned to the following vibrational modes: the totally symmetric ring breathing mode of pyridine, the ethylenic C═C stretch, the CH wag, the pyridine ring C═C stretch, and the ethylenic stretch.[30] The intensity is lower than the one

dx.doi.org/10.1021/jp409844y | J. Phys. Chem. C 2014, 118, 3209−3219

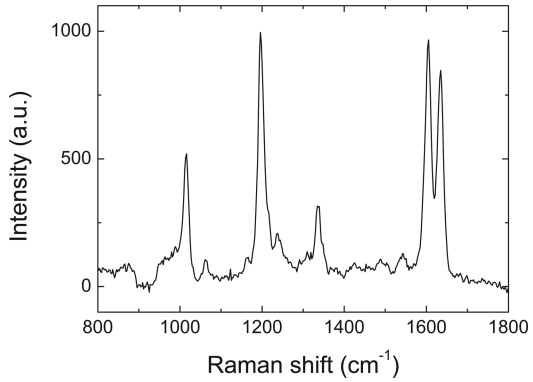

Figure 5. SERS spectrum of BPE acquired on the 10 nm gap dimers sample (laser power 0.49 mW, integration time 30 s).

observed with MB since the cross section of BPE is lower than the one of MB at 785 nm.

3. NUMERICAL MODEL

The electromagnetic scattering problem is governed by Maxwell's equations.[31,32] Only for few target shapes (e.g., spheroids), the analytical solutions of these equations can be retrieved.[33] Therefore, adequate numerical methods should be used to deal with different target shapes. We use the discrete dipole approximation (DDA) that was introduced by DeVoe,[34,35] and Purcell and Pennypacker.[36] The main idea of DDA is to discretize a target shape into a set of N polarizable elements (Figure 6). These elements (called dipoles) get dipole moments and interact together when an electric field is applied. The interdipole distance d (Figure 6) should be chosen to ensure the stability and precision of the method. For this, in a previous study,[37] we compared the DDA results to those of Mie theory for a sphere of radius 40 nm (different values of d were considered). The results showed that an interdipole distance of 1 nm is sufficient to achieve reasonable accuracy for targets of comparable size.

Periodicity. DDA was extended to deal with periodic structures, allowing one to compute the far and near-fields of arrays of periodically reproduced nanoantennas. Reference 38 afforded the problem for 1-D periodic structures, and ref 39 tailored the results to 2-D periodicity. For time consideration, Draine and Flatau[40] introduced a method to compute the dipoles interaction into a periodic lattice. They smoothly suppress the coupling between remote dipoles using a cutoff parameter γ (following an exponential law) that may depend on the periodicity of the structure. For an interparticle distance P = 200 nm, considered in this study (Figure 1), simulations showed that a cutoff parameter γ = 0.1 guarantees accuracy within a reasonable computational time.[41]

Adhesion Layer. Another advantage of the DDA is its ability to deal with any arbitrary shape. Our simulation are carried using DDSCAT 7.1, which is an open source Fortran code.[42,43] We edit the code to define the target dimer antenna with rounded edges and a slanted gap with different inclination angles (Figure 2). The adhesion layer (few nanometers of Cr or Ti typically) used to stick gold on substrate is also taken into account in the model. This layer is usually neglected in simulation even if it broadens the LSPR peak[44−46] as well as the surface plasmon resonance of thin films.[47,48] The role of the adhesion layer is undeniable[49−52] even if some theoretical studies revealed that a chromium layer with thickness smaller than 10 nm only slightly influences the LSPR position for an array of nanocylinders.[45] On the other hand, the adhesion layer plays a crucial role on the plasmonic fluorescence enhancement.[49]

Roughness. The nanofabrication by lithography methods induces a residual roughness on the nanostructures as shown by many AFM[44] or SEM scans.[22,50,53] Usually, the roughness is neglected in numerical models because of the related complexity of implementation. However, a shift between experiments on rough surfaces and simple model calculations are usually observed as mentioned by Reilly et al.[54] Some conventional methods were modified to describe this property of scattering objects: finite difference time domain (FDTD),[55] coupled wave method (CWM),[56] finite element method (FEM),[57,58] boundary element method (BEM),[59] and DDA.[60,61] The comparisons of numerical results with experimental data (for cylindrical antenna) reveal that the modeling of the roughness gives better agreement with experiments.[61]

Our approach consists of generating a smooth target and then altering its surface by removing or adding material pieces from/to the surface.[61] We use a uniform probability law to remove or to add a dipoles from/to the surface or to keep it unchanged (Figure 6). Different roughness levels can be generated by removing or adding more than a unique dipole at once.[61] In the present paper, the roughness is taken into account by adding or removing a unique dipole at once (as the interdipole distance d = 1 nm, the resulting roughness rms = 0.82 nm, which is close to the experimental one varying between 0.4 and 2.4 nm).

Substrate. The DDA is based on the discretization of materials and therefore including the thick substrate is prohibitive using dipoles of the same sizes. Using a model with different size of dipoles can handle the problem; however, it requires huge computational efforts to solve the problem (the fast Fourier transform is no longer applicable in such case[43]).

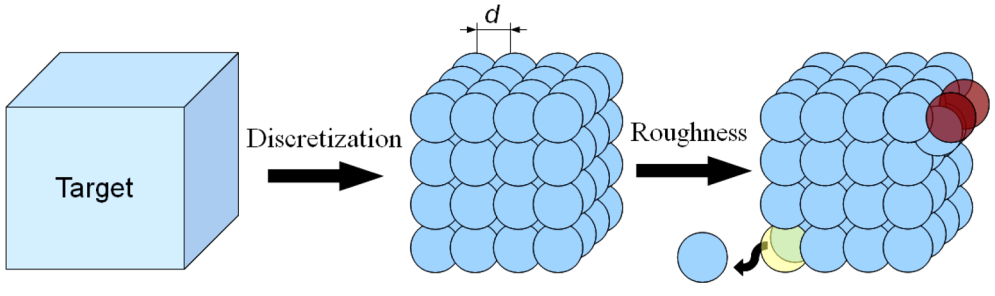

Figure 6. Discretization of the target in a set of dipoles (d interdipole distance) and generation of roughness by adding or removing dipoles.

dx.doi.org/10.1021/jp409844y | J. Phys. Chem. C 2014, 118, 3209−3219

To take into account the substrate contribution in the model, the surrounding mediums (the air and the substrate made of calcium fluoride or quartz, etc.) are modeled by an effective medium.[62,63] We use an effective optical index n_{eff} following the relation proposed by Gehan et al.:[64]

$$n_{eff} = kn_{substrate} + (1 - k)n_{air} \quad (1)$$

where $n_{air} = 1$ and k represents a weighting factor $(0 < k < 1)$ that can be deduced by varying the effective index n_{eff} $(1 < n_{eff} < n_{substrate})$ until matching with the LSPR wavelength obtained experimentally.[64]

The experimental parameters are taken into account including the polarization of incident field along the longitudinal axis of the nanoantenna.[15,65,66] The optical properties of gold and titanium retrieved from refs 67 and 68, and the LSPR position (max $C_{ext}(\lambda)$) is determined with ±5 nm, which gives acceptable precision compared to the measurement uncertainties.[52,69]

The computed LSPR positions match with the experimental ones reported in Table 1 for an effective optical index $n_{eff} = 1.38$ (eq 1, $n_{CaF_2} \approx 1.43$ over the spectral range [500, 950] nm). This value of n_{eff} will be used in the calculations from now on.

Table 1. Experimental and Numerical (DDA with Roughness and for $n_{eff} = 1.38$) LSPR Position λ_{LSPR}

gap G (nm)	experimental λ_{LSPR} (nm)	numerical λ_{LSPR} (nm)
20	710	710
30	705	700
40	688	680
50	686	680

4. EXPERIMENTAL VALIDATION OF THE MODEL (SERS)

Our model[61] has already been validated since it correctly predicts the LSPR position of an array of nanocylinder-based plasmonic sensor. The results showed a better agreement with experiments than other models[45] and fell within the tolerance range deduced from fabrication uncertainties.[69] Here we carry out an experimental validation of our DDA model on gold nanodimers, comparing the predicted SERS properties with experimental measurements.

Experimental Evaluation of the SERS Enhancement Factor. The experimental enhancement factor is evaluated by comparing the SERS signal with the Raman signal measured on a flat gold film (Figure 4, black line), known to provide null or little enhancement, which has undergone the same probe-molecule binding procedure as the antennas.[70,71] The enhancement factor is then given by the ratio of the two signals, normalized to the number of molecules probed in each experiment (N_{SERS} and N_{Raman}). If we assume similar surface coverage (number of molecules binding to gold per unit surface), then the number of probed molecules will be proportional to the gold surface area probed in each experiment, i.e., $N_{SERS} \propto A_{SERS}$ and $N_{Raman} \propto A_{Raman}$. Therefore, the enhancement factor can be estimated by the ratio

$$\begin{aligned} SERS_{EF} &= (I_{SERS}/A_{SERS})/(I_{Raman}/A_{Raman}) \\ &= (I_{SERS}/I_{Raman}) \times (A_{Raman}/A_{SERS}) \end{aligned} \quad (2)$$

where I_{SERS} and I_{Raman} are the SERS and the Raman signals normalized to power and integration time, $A_{Raman} \approx 3.8 \times 10^5$ nm^2 is the area of the gold film illuminated by the laser spot, while $A_{SERS} \approx 3.0 \times 10^5$ nm^2 is the surface area (bound to the molecules) of the dimers that fall within laser spot (ca. six dimers fall within a laser spot of 700 nm diameter). At 785 nm we measure a surface-averaged $SERS_{EF}$ 3.2×10^3. As the signal is lower for BPE, we were not able to measure any Raman signal of BPE on a flat gold film, and then we were not able to calculate precisely the $SERS_{EF}$ for this molecule. However, we assume that we should reach a $SERS_{EF}$ with the same order of magnitude. Notably, we find different values of the enhancement factor when exciting at other wavelengths (660 and 633 nm). The discussion of this effect and its relation to the LSPR position is beyond the scope of this paper.

Numerical Evaluation of the SERS Enhancement Factor. The signal enhancement in SERS results from the interplay between chemical and electromagnetic effects.[3] The electromagnetic contribution is assumed to be more important (whereas the chemical contribution is negligible).[72] It is based on a three-step interaction between a metallic nanostructure and a molecule: (1) at an adequate excitation wavelength λ_{exc}, a significant local enhancement of the electromagnetic field is induced by the metallic particle, (2) this enhanced field excites a molecule in the vicinity of the resonant particle and the molecule scatters a Raman signal, and (3) the Raman signal is enhanced by interaction with the metallic particle (reradiation process[28]) inducing a detectable Raman spectrum. Therefore, the SERS enhancement factor $SERS_{EF}$ is proportional to the product of the field enhancements at λ_{exc} and λ_{Raman}:[73]

$$SERS_{EF} \propto \frac{|E(\lambda_{exc})|^2}{|E_0(\lambda_{exc})|^2} \frac{|E(\lambda_{Raman})|^2}{|E_0(\lambda_{Raman})|^2} \quad (3)$$

where E_0 is the electric field in absence of the metallic nanostructure, $E(\lambda_{exc})$ is the enhanced laser field, and $E(\lambda_{Raman})$ the enhanced reradiated field.

The numerical evaluation of the electromagnetic enhancement factor is based on eq 3, thus neglecting the chemical contribution. For this, the electric field intensity is computed for the excitation and the Raman wavelengths (λ_{exc} and λ_{Raman}) at the surface of the dimer (as no functionalization layer is used to fix the molecules) with a meshing of 1 nm (Figure 10). The excitation laser wavelength λ_{exc} was 785 nm, and the targeted Raman bands are located at 813 nm (Raman shift 445 cm^{-1}) for MB[70,74] and at 902 nm (Raman shift 1200 cm^{-1}) for BPE.[30] The SERS enhancement factor is then deduced for every point of this grid. The detected SERS signal in experiments results from the contribution of all the molecules bonded on the metallic surface of the nanoantenna, although the maximum contribution is expected from the "hot spots" regions, i.e., the points of the nanoantenna where the field enhancement is maximum. Some studies assume SERS results only from the gap contribution (e.g., ref 75). However, this assumption is not verified neither for big molecules of size surpassing the gaps like BSA[46] nor for small gap where only few molecules are entrapped. Moreover, the roughness contributes mostly to the SERS signal when the molecules are directly fixed to the surface (see Figure 10). Therefore, the $SERS_{EF}$ is considered here as the mean value, numerically averaged on the grid points of the surface of the nanoantenna.

Results and Discussion. The SERS enhancement factors, normalized to the smallest gap case (of 10 nm), are displayed in Figure 7. The experimental data as well as the uncertainties on these data (that result from average of data acquired on three

dx.doi.org/10.1021/jp409844y | J. Phys. Chem. C 2014, 118, 3209−3219

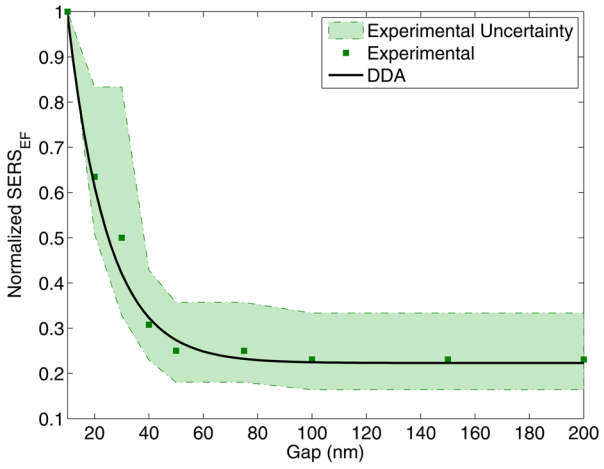

Figure 7. Normalized SERS gain as a function of the gap distance (nm): (a) for MB (λ_{Raman} = 813 nm) and (b) BPE molecules (λ_{Raman} = 902 nm), λ_{exc} = 785 nm.

spectra at different spatial location of the dimers array) are displayed (green dots and green shadow area, respectively). The computed $SERS_{EF}$ (black solid curves) fits well the experimental ones mainly for MB molecule as shown in Figure 7a (for BPE molecule the numerical results overlap the uncertainty domain of experimental data, Figure 7b).

A least-squares fit is carried out on the numerical data using the model $SERS_{EF} = A + B\exp(-G/G_0)$. Here G is the gap and G_0 represents the SERS coupling decay length between the nanords in the dimer antenna, i.e., the distance at which the two nanorods start interacting in the near-field, providing an enhancement of the SERS signal. The following exponential laws were obtained with great agreement with the numerical data (R-squared R^2 = 0.993 for both molecules): $SERS_{EF}$ = 0.223 + 1.52 exp(−G/14.7) for MB molecule (G in nanometers) and $SERS_{EF}$ = 0.168 + 1.73 exp(−G/13.6) for BPE molecule. From the fits we retrieve $G_0 \approx 14$ nm for the SERS coupling decay length.

The exponential law for the SERS gain as a function of the gap can be related to the exponential decay of the LSPR that has been demonstrated in refs 46 and 76−78. The exponential decrease of SERS as a function of the gap size could be justified by the fact that[76] "The resonant plasmons of two Au particles are coupled with each other by photons tunneling through the gap between them. As usual in many other cases of quantum and classical wave tunneling such as evanescent coupling in optical waveguides, the coupling coefficient can be approximated as an exponential function of the gap between them."—in other words, by the decreasing evanescent waves at the surface of the nanoantenna.[79]

The SERS signal is maximum for the smallest investigated gap distance of 10 nm. The exponential behavior (Figure 7) reveals, however, that a much higher SERS signal could be obtained for gaps much smaller than G_0, which is not affordable using the EBL technique (limitation to 5 nm gap). In order to increase the coupling between the two nanoparticles within the dimer and get a more sensitive SERS device, we suggest to modify the gap shape to enhance the SERS.

5. LSPR AND SERS TUNABILITY: EFFECT OF GAP SHAPE AND SLANTING ANGLE

The sensitivity of plasmonic devices to geometrical characteristics makes the SERS substrate tunable. It follows that the performance of such structures could be enhanced by tailoring the geometrical characteristics.

In this section we propose to introduce a new parameter in the design of the nanoantenna. The proposed scheme is to replace the rounded gap obtained by electron beam lithography (Figure 1), by a straight or slanted gap (Figure 2). Before going through simulations for LSPR and SERS, we suggest a sample fabrication method to demonstrate the feasibility of the new shaped gap.

Sample Fabrication. To get nanoantenna with straight or slanted gap, we propose a sample fabrication method following these steps: (i) production of long antenna by EBL of a constant total length for all samples; (ii) introducing gap G (removing some materials) in the antenna by the focused ion beam (FIB) (smooth gap can be achieved by cutting gold segments[25]) or by exploiting the recent advances in helium ion lithography (i.e., ion milling by helium instead of gallium).[26] FIB is able to create nanogaps down to 2 nm wide (difficult to achieve using other lithography techniques).[20] Given these precisions and for comparison with our smallest experimental rounded gap, we assume the gap size of 10 nm (Figure 2). We have fabricated a sample nanoantenna with a gap of 10 nm and slanting angle of 45° based on the two steps described above using FIB (SEM scan shown in Figure 2c). More precision in fabrication could be obtained using the HIL (which is also more costly than FIB).

LSPR Properties. For simulations, we use the same geometrical characteristics and size parameters as reported in the previous section (CaF_2 substrate, 5 nm Ti adhesion layer, w = h = 60 nm, rms = 0.82 nm, and the incident plane wave is polarized along the longitudinal axis of the dimer rods). The total length of the dimer (including the gap G) is set to a constant of 210 nm. The induced gap by FIB is smooth[25] and measures 10 nm (Figure 2). Different slanting angles are considered $\beta \in [0°, 72°]$ (for a total length of 210 nm and a gap of 10 nm, the smallest slanting angle should be below 72°).

The extinction peak amplitude (maximum of extinction spectra, $\max(C_{ext})$) is almost the same for the investigated angles (the variation does not exceed 9.7% as shown by Figure 8). Conversely, when the slanting angle varies from 0° to 72° (and from −72° to 0°, by symmetry consideration), the LSPR peak is significantly red-shifted (ca. 18%, from 785 to 930 nm, as shown in Figure 9), indicating an angle-dependent plasmon

dx.doi.org/10.1021/jp409844y | J. Phys. Chem. C 2014, 118, 3209−3219

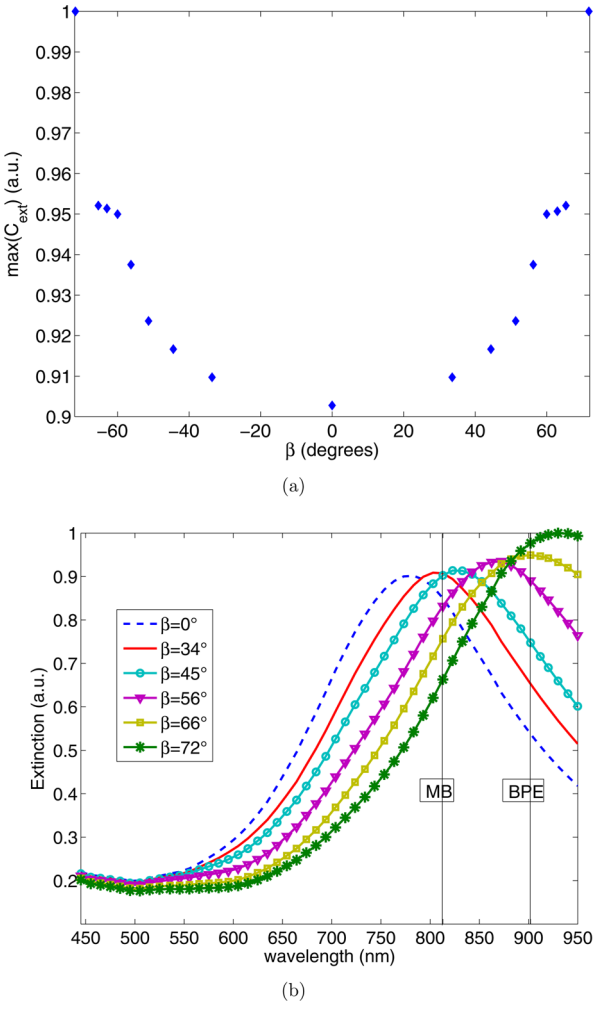

Figure 8. Extinction (au) as a function of the slanting angle β: (a) extinction peak amplitude (au); (b) extinction spectra (the Raman wavelength of MB (λ_{Raman} = 813 nm) and BPE (λ_{Raman} = 902 nm), under λ_{exc} = 785 nm are highlighted by vertical lines as a guide to the eye).

coupling.[76] Therefore, varying the slanting angle enables tuning of the position of the LSPR by preserving its quality factor.

The dependence on the angle and gap can be fitted using an exponential law,[46,76,78] known as the plasmon ruler equation.[77,80] The validity of this equation was investigated in some previous studies. Funston et al.[78] found that the exponential fit is no more valid for small ratio of gap by rod length and concluded that the exponential law serves only as empirical approximation. In that case the investigated gap was smaller than 2 nm. Similar conclusions for 2D arrays of nanospheres were driven by Ben and Park and qualitatively interpreted.[81]

In our case, we can use the plasmon ruler equation.[78] However, instead of using the effective gap G = 10 nm, we use $G/\cos(\beta)$ which represents the gap perceived by the electric field polarized along the antenna long axis (Figure 2). The least-squares fit yields the following equation with R^2 = 0.998:

$$\frac{\Delta\lambda_{LSPR}}{\lambda_{LSPR}(\beta = 0°)} = 0.226 - 0.496 \exp\left(-\frac{1}{12.8}\frac{G}{\cos(\beta)}\right) \quad (4)$$

This equation shows that when the gap perceived by the electric field $G/\cos(\beta)$ increases, the plasmon is red-shifted,

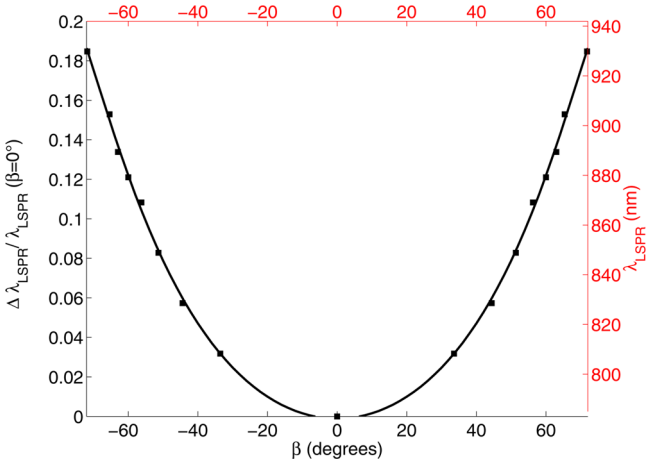

Figure 9. Relative LSPR position variation $\Delta\lambda_{LSPR}/\lambda_{LSPR}(\beta = 0°)$ and LSPR position λ_{LSPR} (nm) as a function of the slanting angle β (squares represent the numerical data, and the solid curve represents their interpolation by exponential law).

indicating more coupling between the nanoantenna. Given the constant effective gap distance G, such behavior can be associated with the area of the gap sides: the coupling induced by the important charge density on both sides of the surface of the gap[82] increases when the area of these sides increases (i.e., when β increases). Thus, the LSPR shift may depend not only on the gap distance but also on the area of gap sides.

Near-Field and SERS Enhancement. The straight gap (β = 0°) enables more coupling between the two antennas than the rounded gap as it induces an improvement of the near-field by 1 order of magnitude (Figure 10, the intensity in logarithmic

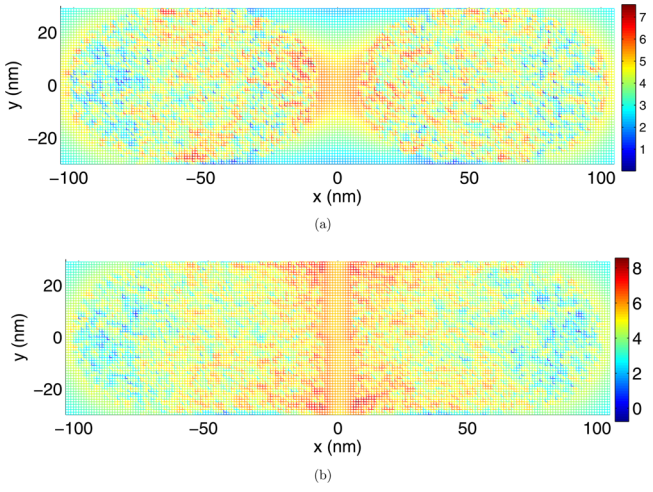

Figure 10. Normalized relative near-field intensity in logarithmic scale $\log(|E|^2/|E_0|^2)$, computed in a plane 1 nm above the mean surface of the nanoantenna (for λ_{exc} = 785 nm): (a) nanoantenna with rounded gap; (b) nanoantenna with straight gap. The observed nonuniformity of near-field distribution is due to the roughness of the nanoparticle surface.

scale shows that the enhancement reaches 8 for straight gap versus 7 for rounded gap). This field coupling can be explained by much more concentrated charges on both sides of the surface of the straight gap.

In order to gain insight into how much the slanting angle affects the SERS, we calculate the mean value of the relative

dx.doi.org/10.1021/jp409844y | J. Phys. Chem. C 2014, 118, 3209−3219

field intensity (surface-averaged cf. subsection 4.2) and then the SERS enhancement factor for different slanting angles β.

The mean value of the relative field intensity enhancement mean($|E|^2/|E_0|^2$) for the different slanting angles is displayed in Figure 11. It reaches its highest value at λ_{Raman}(MB) and

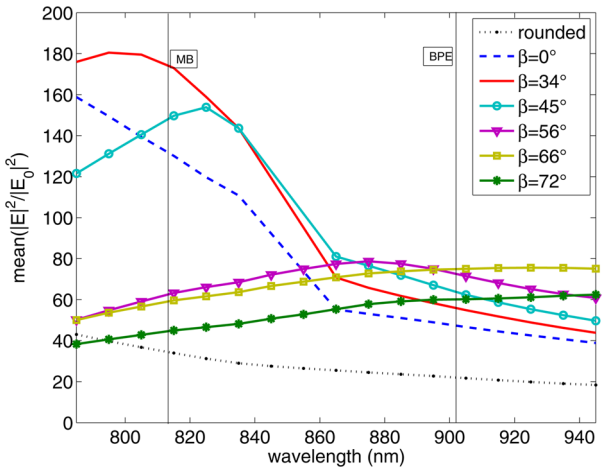

Figure 11. Mean value of the relative field intensity (mean($|E|^2/|E_0|^2$)) as a function of wavelength (λ) for rounded gap and slanted gap with different slanting angles β. The Raman wavelengths of MB (λ_{Raman} = 813 nm) and BPE (λ_{Raman} = 902 nm) are highlighted by vertical lines as a guide to the eye.

λ_{Raman}(BPE) for slanting angles of 34° and 66°, respectively. It should be noticed that the LSPR position is closest to λ_{Raman}(MB) and λ_{Raman}(BPE) for these angles, respectively (Figure 8b). For better SERS detection, the near-field should be maximal for the excitation wavelength λ_{exc} and the Raman wavelength λ_{Raman}. The mean value of near field, as an indicator of the SERS behavior, shows that the slanting angle should be around 34° for a better detection of the MB molecule, since the slanting angle of 34° ensures the highest near-field enhancement at λ_{exc} set to 785 nm for all simulations (Figure 11). The slanting angle β = 66°, ensuring the best near-field enhancement at λ_{Raman}(BPE), does not ensure high field enhancement at λ_{exc}. Therefore, the SERS behavior cannot be clearly anticipated from the near-field data for BPE molecule.

The relative SERS enhancement factors are displayed in logarithmic scale in Figure 12, assuming excitation wavelength λ_{exc} = 785 nm, and show important improvements with the new design of gap. The straight gap (blue dashed curve) allows a greater $SERS_{EF}$ by at least 1 order of magnitude compared to the one obtained with rounded gap (black dotted curve). Slanting angles below 66° (red, cyan, magenta, and yellow curves) allow a greater $SERS_{EF}$ by at least 3 times compared to what obtained for rounded gap. Moreover, the highest $SERS_{EF}$ is reached for a slanting angle β = 34°. For this angle, the relative SERS enhancement factor is of the order of 10^5, which is about 20 times greater than the one obtained assuming rounded gap (of the order of 10^3–10^4 over the investigated spectral range): For MB molecule: relative $SERS_{EF}$ = 3.5 × 10^3 for rounded gap versus a relative $SERS_{EF}$ = 200 × 10^3 for a slanted gap β = 34° (about 57 times greater). For BPE molecule: relative $SERS_{EF}$ = 1.78 × 10^3 for rounded gap versus a relative $SERS_{EF}$ = 32.15 × 10^3 for a slanted gap β = 34° (about 18 times greater). Finally, the relative computed surface-averaged $SERS_{EF}$ reaches up to 2.5 × 10^5, which is greater than that found for some recently designed SERS substrates (e.g., Le

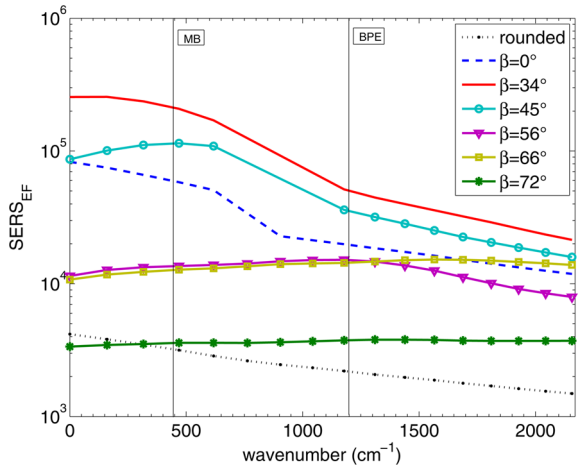

Figure 12. Relative SERS enhancement factor $SERS_{EF}$ as a function of the wavenumber under excitation wavelength λ_{exc} = 785 nm for rounded gap and slanted gap with different slanting angles β. The targeted Raman bands of MB (445 cm^{-1}) and BPE (1200 cm^{-1}) are highlighted by vertical lines as a guide to the eye.

Ru et al. reported 4.8 × 10^4,[83] Li et al. reported 2 × 10^4,[25] and Alexander et al. reported an enhancement of the order 10^5 considering only the gap region[75]).

6. CONCLUSIONS

In this study we focused on improving the SERS of dimer antenna (near-field coupled nanorods) by changing the gap geometry. Our numerical model (DDA for periodic rough structures) was first validated on a set of SERS experiments on dimer antenna 100 × 60 × 60 ($L \times w \times h$) on CaF_2 substrates with rounded gap, on two molecules MB and BPE. The experiments and numerical results reveal for two different molecules that the SERS signal gets increased when the gap decreases, which has technical limitations. Therefore, to enhance the sensitivity of the dimer, we suggest a new shape of the gap: a straight or slanted gap which can be fabricated (cf. subsection 5.1).

Simulations were carried out to determine the dependence of the LSPR (extinction peak) and the SERS on the slanting angle for gold nanoantenna dimers. Our main findings are:

1. The LSPR shift with respect to the straight gap can be as large as 145 nm and can be fitted using an extended formulation of the plasmon ruler equation (with almost the same level of extinction).

2. A stronger coupling between the antennas can be achieved using a slanted gap, leading to a more enhanced near-field. The resulting near-field intensity maximal value is greater by 1 order of magnitude for straight gap compared to the rounded gap.

3. The SERS enhancement factor can be maximized by changing the slanting angle. For adequate gap slanting angle, the SERS enhancement factor can be approximately 20 times greater than the one obtained for the rounded gap and can be up to 2 orders of magnitude. With such improvements, a higher sensitivity of the device may be achieved.

■ ASSOCIATED CONTENT

Supporting Information

Full list of authors of references with more than 10 authors. This material is available free of charge via the Internet at http://pubs.acs.org.

dx.doi.org/10.1021/jp409844y | J. Phys. Chem. C 2014, 118, 3209–3219

AUTHOR INFORMATION

Corresponding Author

*E-mail: samehkessentini@gmail.com (S.K.).

Notes

The authors declare no competing financial interest.

ACKNOWLEDGMENTS

The authors thank the Nanoantenna European Project (FP7 Health-F5-2009-241818), the Région Champagne-Ardennes, the Conseil Régional de l'Aube, and MIUR (Project PRIN 2008J858Y7 and Programma Operativo Nazionale Ricerca e Competitivitá 2007-2013, PON01_01322 PANREX) for financial support.

REFERENCES

(1) http//www.nanoantenna.eu/.

(2) Brolo, A. G. Plasmonics for Future Biosensors. *Nat. Photonics* **2012**, *6*, 709−713.

(3) Ru, E. C. L.; Etchegoin, P. G. *Principles of Surface-Enhanced Raman Spectroscopy and Related Plasmonic Effects*; Elsevier: Cambridge, 2009.

(4) Schlücker, S. SERS Microscopy: Nanoparticle Probes and Biomedical Applications. *ChemPhysChem* **2009**, *10*, 1344−1354.

(5) Guillot, N.; Lamy de la Chapelle, M. Lithographied Nanostructures as Nanosensors. *J. Nanophotonics* **2012**, *6*, 1−28.

(6) Guillot, N.; Lamy de la Chapelle, M. The Electromagnetic Effect in Surface Enhanced Raman Scattering: Enhancement Optimization Using Precisely Controlled Nanostructures. *J. Quant. Spectrosc. Radiat. Transfer* **2012**, *113*, 2321−2333.

(7) Svedberg, F.; Li, Z.; Xu, H.; Kall, M. Creating Hot Nanoparticle Pairs for Surface-Enhanced Raman Spectroscopy Through Optical Manipulation. *Nano Lett.* **2006**, *6*, 2639−2641.

(8) Messina, E.; Cavallaro, E.; Cacciola, A.; Saija, R.; Borghese, F.; Denti, P.; Fazio, B.; D'Andrea, C.; Gucciardi, P. G.; Iatí, M. A.; et al. Manipulation and Raman Spectroscopy with Optically Trapped Metal Nanoparticles Obtained by Pulsed Laser Ablation in Liquids. *J. Phys. Chem. C* **2011**, *115*, 5115−5122.

(9) Hao, E.; Schatz, G. C. Electromagnetic Fields around Silver Nanoparticles and Dimers. *J. Chem. Phys.* **2004**, *120*, 357−346.

(10) Zou, S.; Schatz, G. C. Silver Nanoparticle Array Structures That Produce Giant Enhancements in Electromagnetic Fields. *Chem. Phys. Lett.* **2005**, *403*, 62−67.

(11) Nie, S.; Emory, S. R. Probing Single Molecules and Single Nanoparticles by Surface-Enhanced Raman Scattering. *Science* **1997**, *275*, 1102−1106.

(12) Kneipp, K.; Wang, Y.; Kneipp, H.; Perelman, L. T.; Itzkan, I.; Dasari, R. R.; Feld, M. S. Single Molecule Detection Using Surface-Enhanced Raman Scattering. *Phys. Rev. Lett.* **1997**, *78*, 1667−1670.

(13) Guillot, N.; Shen, H.; Fremaux, B.; Pron, O.; Rinnert, E.; Toury, T.; Lamy de la Chapelle, M. Surface Enhanced Raman Scattering Optimization of Gold Nanocylinder Arrays: Influence of the Localized Surface Plasmon Resonance and Excitation Wavelength. *Appl. Phys. Lett.* **2010**, *97*, 023113.

(14) Billot, L.; Lamy de la Chapelle, M.; Grimault, A.-S.; Vial, A.; Barchiesi, D.; Bijeon, J.-L.; Adam, P.-M.; Royer, P. Surface Enhanced Raman Scattering on Gold Nanowire Arrays: Evidence of Strong Multipolar Surface Plasmon Resonance Enhancement. *Chem. Phys. Lett.* **2006**, *422*, 303−307.

(15) Grand, J.; Lamy de la Chapelle, M.; Bijeon, J.-L.; Adam, P.-M.; Vial, A.; Royer, P. Role of Localized Surface Plasmons in Surface Enhanced Raman Scattering of Shape-Controlled Metallic Particles in Regular Arrays. *Phys. Rev. B* **2005**, *72*, 1−4.

(16) Fischer, H.; Martin, O. J. F. Engineering the Optical Response of Plasmonic Nanoantennas. *Opt. Express* **2008**, *16*, 9144−9154.

(17) Smythe, E. J.; Cubukcu, E.; Capasso, F. Optical Properties of Surface Plasmon Resonances of Coupled Metallic Nanorods. *Opt. Express* **2007**, *15*, 7439−7447.

(18) Qiu, T.; Zhang, W.; Chu, P. K. Recent Progress in Fabrication of Anisotropic Nanostructures for Surface-Enhanced Raman Spectroscopy. *Recent Pat. Nanotechnol.* **2009**, *3*, 10−20.

(19) Ratto, F.; Matteini, P.; Rossi, F.; Pini, R. Size and Shape Control in the Overgrowth of Gold Nanorods. *J. Nanopart. Res.* **2010**, *12*, 2029−2036.

(20) Langford, R. M.; Nellen, P. M.; Gierak, J.; Fu, Y. Focused Ion Beam Micro- and Nanoengineering. *MRS Bull.* **2007**, *32*, 417−423.

(21) Gopinath, A.; Boriskina, S. V.; Premasiri, W. R.; Ziegler, L.; Reinhard, B. M.; Negro, L. D. Plasmonic Nanogalaxies: Multiscale Aperiodic Arrays for Surface-Enhanced Raman Sensing. *Nano Lett.* **2009**, *9*, 3922−3929.

(22) Tabor, C.; Haute, D. V.; El-Sayed, M. A. Effect of Orientation on Plasmonic Coupling Between Gold Nanorods. *ACS Nano* **2009**, *11*, 3670−3678.

(23) Banaee, M. G.; Crozier, K. B. Mixed Dimer Double-Resonance Substrates for Surface-Enhanced Raman Spectroscopy. *ACS Nano* **2011**, *5*, 307−314.

(24) Yue, W.; Yang, Y.; Wang, Z.; Chen, L.; Wang, X. Surface-Enhanced Raman Scattering on Gold Nanorod Pairs with Interconnection Bars of Different Widths. *Sens. Actuators, B* **2012**, *171−172*, 734−738.

(25) Li, S.; Pedano, M. L.; Chang, S.-H.; Mirkin, C. A.; Schatz, G. C. Gap Structure Effects on Surface-Enhanced Raman Scattering Intensities for Gold Gapped Rods. *Nano Lett.* **2010**, *10*, 1722−1727.

(26) Melli, M.; Polyakov, A.; Gargas, D.; Huynh, C.; Scipioni, L.; Bao, W.; Ogletree, D. F.; Schuck, P. J.; Cabrini, S.; Weber-Bargioni, A. Reaching the Theoretical Resonance Quality Factor Limit in Coaxial Plasmonic Nanoresonators Fabricated by Helium Ion Lithography. *Nano Lett.* **2013**, *13*, 2687−2691.

(27) Kessentini, S.; Barchiesi, D. Effect of Gap Shape on the Spectral Response and Field Enhancement of Dimer-Based Biosensor. *PIERS Proceedings. Moscow and Russia*, 2012; pp 24−28.

(28) Fazio, B.; D'Andrea, C.; Bonaccorso, F.; Irrera, A.; Calogero, G.; Vasi, C.; Gucciardi, P. G.; Allegrini, M.; Toma, A.; Chiappe, D.; et al. Re-radiation Enhancement in Polarized Surface-Enhanced Resonant Raman Scattering of Randomly Oriented Molecules on Self-Organized Gold Nanowires. *ACS Nano* **2011**, *5*, 5945−5956.

(29) Aoki, P. H.; Volpati, D.; Caetano, W.; Constantino, C. J. Study of the Interaction Between Cardiolipin Bilayers and Methylene Blue in Polymer-Based Layer-by-Layer and Langmuir Films Applied as Membrane Mimetic Systems. *Vib. Spectrosc.* **2010**, *54*, 93−102.

(30) Yang, W.-H.; Hulteen, J.; Schatz, G. C.; Duyne, R. V. A Surface-Enhanced Hyper-Raman and Surface-Enhanced Raman Scattering Study of Trans-1,2-bis(4-pyridyl)ethylene Adsorbed onto Silver Film over Nanosphere Electrodes. Vibrational Assignments: Experiment and Theory. *J. Chem. Phys.* **1996**, *104*, 4313−4323.

(31) Kahnert, F. M. Numerical Method in Electromagnetic Scattering Theory. *J. Quant. Spectrosc. Radiat. Transfer* **2003**, *79−80*, 775−824.

(32) Borghese, F.; Saija, R.; Gucciardi, P. G.; Iati, M. A.; Maragó, O. M. Electromagnetic and Light Scattering by Non-Spherical Particles XIII. *J. Quant. Spectrosc. Radiat. Transfer* **2012**, *113*, 2277−2608.

(33) Guzatov, D. V.; Klimov, V. V. Optical Properties of a Plasmonic Nano-Antenna: An Analytical Approach. *New J. Phys.* **2011**, *13*, 053034.

(34) Devoe, H. Optical Properties of Molecular Aggregates. I. Classical Model of Electronic Absorption and Refraction. *J. Chem. Phys.* **1964**, *41*, 393−400.

(35) Devoe, H. Optical Properties of Molecular Aggregates. II. Classical Theory of the Refraction and Absorption and Optical Activity of Solutions and Crystals. *J. Chem. Phys.* **1965**, *43*, 3199−3208.

(36) Purcell, E.; Pennypacker, C. R. Scattering and Absorption of Light by Nonspherical Dielectric Grains. *Astron. J.* **1973**, *186*, 705−714.

(37) Kessentini, S.; Barchiesi, D. Quantitative Comparison of Optimized Nanorods and Nanoshells and Hollow Nanospheres for Photothermal Therapy. *Biomed. Opt. Express* **2012**, *3*, 590−604.

(38) Markel, V. A. Coupled-Dipole Approach to Scattering of Light from a One-Dimensional Periodic Dipole Structure. *J. Mod. Opt.* **1993**, *40*, 2281−2291.
(39) Chaumet, P. C.; Rahmani, A.; Bryant, G. W. Generalization of the Coupled Dipole Method to Periodic Structures. *Phys. Rev. B* **2003**, *67*, 165404(1−5).
(40) Draine, B. T.; Flatau, P. J. Discrete-Dipole Approximation for Periodic Targets Theory and Tests. *J. Opt. Soc. Am. A* **2008**, *25*, 2693−2703.
(41) Kessentini, S. Modeling and Optimization of Plasmonic Nanostructures: Biomedical Applications. Ph.D. Thesis, University of Technology of Troyes, 2012.
(42) Draine, B. T.; Flatau, P. J. User Guide to the Discrete Dipole Approximation Code DDSCAT 7.1. http//arXiv.org/abs/1002.1505v1, 2010.
(43) Draine, B. T.; Flatau, P. J. Discrete-Dipole Approximation for Scattering Calculations. *J. Opt. Soc. Am. A* **1994**, *11*, 1491−1499.
(44) Zheng, Y. B.; Juluri, B. K.; Mao, X.; Walker, T. R.; Huang, T. J. Systematic Investigation of Localized Surface Plasmon Resonance of Long-Range Ordered Au Nanodisk Arrays. *J. Appl. Phys.* **2008**, *103*, 1−9.
(45) Vial, A.; Laroche, T. Description of Dispersion Properties of Metals by Means of the Critical Points Model and Application to the Study of Resonant Structures Using the FDTD Method. *J. Phys. D: Appl. Phys.* **2007**, *40*, 7152−7158.
(46) Aćimović, S. S.; Kreuzer, M. P.; González, M. U.; Quidan, R. Plasmon Near-Field Coupling in Metal Dimers as a Step Toward Single-Molecule Sensing. *ACS Nano* **2009**, *3*, 1231−1237.
(47) Barchiesi, D.; Lidgi-Guigui, N.; Lamy de la Chapelle, M. Functionalization Layer Influence on the Sensitivity of Surface Plasmon Resonance (SPR) Biosensor. *Opt. Commun.* **2012**, *285*, 1619−1623.
(48) Barchiesi, D. In *Numerical Optimization of Plasmonic Biosensors*; Serra, P. P. A., Ed.; INTECH and Open Access Publisher: 2011; Vol. 4.
(49) Aouani, H.; Wenger, J.; Gérard, D.; Rigneault, H.; Devaux, E. T. W.; Ebbesen, F. M.; Xu, T.; Blair, S. Crucial Role of the Adhesion Layer on the Plasmonic Fluorescence Enhancement. *ACS Nano* **2009**, *3*, 2043−2048.
(50) Shen, H.; Guillot, N.; Rouxel, J.; Lamy de la Chapelle, M.; Toury, T. Optimized Plasmonic Nanostructures for Improved Sensing Activities. *Opt. Express* **2012**, *20*, 21278−21290.
(51) Lamy de la Chapelle, M.; Shen, H.; Guillot, N.; Frémaux, B.; Guelorget, B.; Toury, T. New Gold Nanoparticles Adhesion Process Opening the Way of Improved and Highly Sensitive Plasmonics Technologies. *Plasmonics* **2012**, 1−5.
(52) Kessentini, S.; Barchiesi, D. In *Nanostructured Biosensors: Influence of Adhesion Layer, Roughness and Size on the LSPR: A Parametric Study*; Rinken, T., Ed.; INTECH and Open Access Publisher, 2013.
(53) Kumar, A.; Fung, K. H.; Fang, N. X. Probing Surface-Plasmon Hybridization Using Cathodoluminescence. *Nanotechnology* **2011**, *22*, 155302 (1−6).
(54) Reilly, T. H.; Chang, S. H.; Corbman, J. D.; Schatz, G. C.; Rowlen, K. L. Quantitative Evaluation of Plasmon Enhanced Raman Scattering from Nanoaperture Arrays. *J. Phys. Chem. C* **2007**, *111*, 1689−1694.
(55) Hastings, F. D.; Schneider, J. B.; Broschat, S. L. A Monte-Carlo FDTD Technique for Rough Surface Scattering. *IEEE Trans. Antennas Propagat.* **1995**, *43*, 1183−1191.
(56) Byun, K. M.; Yoon, S. J.; Kim, D.; Kim, S. J. Sensitivity Analysis of a Nanowire-Based Surface Plasmon Resonance Biosensor in the Presence of Surface Roughness. *J. Opt. Soc. Am. A* **2007**, *24*, 522−529.
(57) Poroshin, V.; Borovin, Y.; Bogomolov, D. Transfer of the Surface Roughness Geometry Into the Universal FEM Software ANSYS. *Adv. Eng.* **2009**, *3*, 231−236.
(58) Kato, A.; Burger, S.; Scholze, F. Analytical Modeling and Three-Dimensional Finite Element Simulation in Line Edge Roughness in Scatterometry. *Appl. Opt.* **2012**, *51*, 6457−6464.
(59) Trügler, A.; Tinguely, J.-C.; Krenn, J. R.; Hohenau, A.; Hohenester, U. Influence of Surface Roughness on the Optical Properties of Plasmonic Nanoparticles. *Phys. Rev. B* **2011**, *83*, 1−4.
(60) Parviainen, H.; Lumme, K. Light Scattering from Rough Thin Films DDA Simulations. *ICHMT Digital Library Online* **2007**, *14*, 153−156.
(61) Kessentini, S.; Barchiesi, D. Roughness Effect on the Efficiency of Dimer Antenna Based Biosensor. *AEM* **2012**, *1*, 41−47.
(62) Haija, A. J.; Freeman, W. L.; Roarty, T. Effective Characteristic Matrix of Ultrathin Multilayer Structures. *Opt. Appl.* **2006**, *36*, 39−50.
(63) Pelton, M.; Aizpurua, J.; Bryant, G. W. Metal-Nanoparticles Plasmonics. *Laser Photonics Rev.* **2008**, *2*, 136−159.
(64) Gehan, H.; Mangeney, C.; Aubard, J.; Levi, G.; Hohenau, A.; Krenn, J. R.; Lacaze, E.; Félidj, N. Design and Optical Properties of Active Polymer-Coated Plasmonic Nanostructures. *J. Phys. Chem. Lett.* **2011**, *2*, 926−931.
(65) Messina, E.; Cavallaro, E.; Cacciola, A.; Iatí, M. A.; Gucciardi, P. G.; Borghese, F.; Denti, P.; Saija, R.; Compagnini, G.; Meneghetti, M.; et al. Plasmon-Enhanced Optical Trapping of Gold Nanoaggregates with Selected Optical Properties. *ACS Nano* **2011**, *5*, 905−913.
(66) Guo, R.; Kinzel, E. C.; Li, Y.; Uppuluri, S. M.; Raman, A.; Xu, X. Three-Dimensional Mapping of Optical Near Field of a Nanoscale Bowtie Antenna. *Opt. Express* **2010**, *18*, 4961−4971.
(67) Johnson, P. B.; Christy, R. W. Optical Constants of the Noble Metals. *Phys. Rev. B* **1972**, *6*, 4370−4379.
(68) Johnson, P. B.; Christy, R. W. Optical Constants of Transition Metals: Ti and V and Cr and Mn and Fe and Co and Ni and Pd. *Phys. Rev. B* **1974**, *9*, 5056−5070.
(69) Barchiesi, D.; Kessentini, S.; Guillot, N.; Lamy de la Chapelle, M.; Grosges, T. Localized Surface Plasmon Resonance in Arrays of Nano-Gold Cylinders: Inverse Problem and Propagation of Uncertainties. *Opt. Express* **2013**, *21*, 2245−2262.
(70) D'Andrea, C.; Bochterle, J.; Toma, A.; Huck, C.; Neubrech, F.; Messina, E.; Fazio, B.; Marago, O. M.; Di Fabrizio, E.; Lamy de la Chapelle, M.; et al. Optical Nanoantennas for Multiband Surface-Enhanced Infrared and Raman Spectroscopy. *ACS Nano* **2013**, *17*, 3522−3531.
(71) Ru, E. C. L.; Meyer, S. A.; Artur, C.; Etchegoin, P. G.; Grand, J.; Lang, P.; Maurel, F. Experimental Demonstration of Surface Selection Rules for SERS on Flat Metallic Surfaces. *Chem. Commun.* **2011**, *47*, 3903−3905.
(72) Nie, S.; Emory, S. R. Probing Single Molecules and Single Nanoparticles by Surface-Enhanced Raman Scattering. *Science* **1997**, *275*, 1102−1106.
(73) Wokaun, A. Surface Enhanced Electromagnetic Processes. *Solid State Phys.* **1984**, *38*, 223−293.
(74) Naujok, R. R.; Duevel, R. V.; Corn, R. M. Fluorescence and Fourier Transform Surface-Enhanced Raman Scattering Measurements of Methylene Blue Adsorbed Onto a Sulfur-Modified Gold Electrode. *Langmuir* **1993**, *9*, 1771−1774.
(75) Alexander, K. D.; Skinner, K.; Zhang, S.; Wei, H.; Lopez, R. Tunable SERS in Gold Dimers Through Strain Control on Elastometric Substrate. *Nano Lett.* **2010**, *10*, 4488−4493.
(76) Su, K.-H.; Wei, Q.-H.; Zhang, X.; Mock, J. J.; Smith, D. R.; Schultz, S. InterParticle Coupling Effects on Plasmon Resonances of Nanogold Particles. *Nano Lett.* **2003**, *3*, 10871090.
(77) Jain, P. K.; Huang, W.; El-Sayed, M. A. On the Universal Scaling Behavior of the Distance Decay of Plasmon Coupling in Metal Nanoparticle Pairs: A Plasmon Ruler Equation. *Nano Lett.* **2007**, *7*, 2080−2088.
(78) Funston, A. M.; Novo, C.; Davis, T. J.; Mulvaney, P. Plasmon Coupling of Gold Nanorods at Short Distances and in Different Geometries. *Nano Lett.* **2009**, *9*, 1651−1658.
(79) Barchiesi, D.; Grosges, T. Measurement of Decay Lengths of Evanescent Waves The Lock-in Non Linear Filtering. *New J. Phys.* **2006**, *8*, 263−273.
(80) Reinhard, B. M.; Siu, M.; Agarwal, H.; Alivisatos, A. P.; Liphardt, J. Calibration of Dynamic Molecular Rulers Based on Plasmon

Coupling Between Gold Nanoparticles. *Nano Lett.* **2005**, *5*, 2246−2252.
(81) Ben, X.; Park, H. S. Size Dependence of the Plasmon Ruler Equation for Two-Dimensional Metal Nanosphere Arrays. *J. Phys. Chem. C* **2011**, *115*, 15915−15926.
(82) Kottmann, J.; Martin, O. Retardation-Induced Plasmon Resonances in Coupled Nanoparticles. *Opt. Lett.* **2001**, *26*, 1096−1098.
(83) Ru, E. C. L.; Grand, J.; Sow, I.; Somerville, W. R. C.; Etchegoin, P. G.; Treguer-Delapierre, M.; Charron, G.; Félidj, N.; Lévi, G.; Aubard, J. A Scheme for Detecting Every Single Target Molecule with Surface-Enhanced Raman Spectroscopy. *Nano Lett.* **2011**, *11*, 5013−5019.